Published in final edited form as:
Nat Med. 2015 October ; 21(10): 1182–1189. doi:10.1038/nm.3955.

Metabolic reprogramming induces resistance to anti-NOTCH1 therapies in acute lymphoblastic leukemia

Daniel Herranz[1], **Alberto Ambesi-Impiombato**[1], **Jessica Sudderth**[2], **Marta Sánchez-Martín**[1], **Laura Belver**[1], **Valeria Tosello**[1,#], **Luyao Xu**[1], **Agnieszka A. Wendorff**[1], **Mireia Castillo**[3], **J. Erika Haydu**[1], **Javier Márquez**[4], **José M. Matés**[4], **Andrew L. Kung**[5], **Stephen Rayport**[6], **Carlos Cordon-Cardo**[3], **Ralph J. DeBerardinis**[2], and **Adolfo A. Ferrando**[1,5,7,†]

[1]Institute for Cancer Genetics, Columbia University, New York, NY, 10032, USA

[2]Children's Medical Center Research Institute, University of Texas-Southwestern Medical Center, Dallas, TX, USA

[3]Department of Pathology, Icahn School of Medicine at Mount Sinai, New York, NY, USA

[4]Department of Molecular Biology and Biochemistry, Faculty of Sciences, Campus de Teatinos, University of Málaga-Instituto de Investigación Biomédica de Málaga, Málaga, Spain

[5]Department of Pediatrics, Columbia University Medical Center, New York, NY, USA

[6]Department of Psychiatry, Columbia University Medical Center, New York, NY, USA

[7]Department of Pathology, Columbia University Medical Center, New York, NY, USA

Abstract

Activating mutations in *NOTCH1* are common in T-cell acute lymphoblastic leukemia (TALL). Here we identify glutaminolysis as a critical pathway for leukemia cell growth downstream of NOTCH1 and a key determinant of clinical response to anti-NOTCH1 therapies. Mechanistically, inhibition of NOTCH1 signaling in T-ALL induces a metabolic shutdown with prominent inhibition of glutaminolysis and triggers autophagy as a salvage pathway supporting leukemia cell metabolism. Consequently, both inhibition of glutaminolysis and inhibition of autophagy strongly

[†]Corresponding author: Contact Information: Adolfo A. Ferrando, Associate Professor of Pediatrics and Pathology, Institute for Cancer Genetics, Columbia University Medical Center, New York, NY, USA, Phone: 212-851-4611, FAX: 212-851-5256, af2196@columbia.edu.
[#]Current address: Istituto Oncologico Veneto, Istituto di Ricovero e Cura a Carattere Scientifico, Padua, Italy.

ACCESSION CODES

Microarray gene expression data are available in Gene Expression Omnibus (GEO) under accession codes GSE71087 and GSE71089.

AUTHOR CONTRIBUTIONS

D.H. carried out most of the experiments. A.A.I. analyzed gene expression profile signatures. J.S. performed metabolic studies. M.S.M performed some *in vivo* and *in vitro* drug response analyses. L.B. analyzed PTEN levels by intracellular FACS staining. V.T. generated NOTCH1-induced primary leukemias. L.X. performed some animal studies with D.H. A.A.W. performed some experiments with human primary T-ALL samples. M.C. conducted histological evaluation of tumor development and response to therapy. E.H. performed some *in vivo* experiments. J.M. and J.M.M. contributed reagents. S.R. generated the *Gls* conditional knockout mice. A.L.K. conceived and supervised bioimaging studies. C.C-C. supervised histological analyses. R.J.D. supervised metabolic isotope tracing analyses. A.A.F designed the study, supervised research and wrote the manuscript with D.H.

COMPETING FINANTIAL INTERESTS

The authors declare no competing financial interests.

and synergistically enhance the antileukemic effects of anti-NOTCH1 therapies. Moreover, we demonstrate that *Pten* loss induces increased glycolysis and consequently rescues leukemic cell metabolism abrogating the antileukemic effects of NOTCH1 inhibition. Overall, these results identify glutaminolysis as a major node in cancer metabolism controlled by NOTCH1 and as therapeutic target for the treatment of T-ALL.

NOTCH signaling is a conserved signal transduction pathway with a prominent role in cell differentiation and tissue patterning during development[1]. In the hematopoietic system, NOTCH1 has been implicated in stem cell homeostasis and most prominently as a major driver of T-cell lineage specification in lymphoid progenitors and a master regulator of thymocyte development[2–4]. In addition, aberrant NOTCH1 signaling plays a major role in the pathogenesis of over 60% of T-ALLs harboring activating mutations in the *NOTCH1* gene[5]. Most notably, oncogenic NOTCH1 has been proposed as a therapeutic target in *NOTCH1*-mutant leukemias and small molecule γ-secretase inhibitors (GSIs), which effectively block NOTCH activation via inhibition of a critical intramembrane proteolytic cleavage required for NOTCH signaling[6], are now in clinical development for the treatment of relapsed and refractory T-ALL. However, the clinical development of anti-NOTCH1 therapies in T-ALL has been hampered by the limited and delayed therapeutic response to these drugs, making the identification of highly effective and synergistic drug combinations capable of delivering strong antileukemic responses a top priority in the field. In addition, and most troubling, most T-ALL cell lines harboring activating mutations in *NOTCH1* fail to respond to GSI therapy, a phenotype strictly associated with mutational loss of the Phophatase and tensin homolog (*PTEN*) tumor suppressor gene[7], making essential to establish the specific role and mechanisms of *PTEN* inactivation as driver of resistance to anti-NOTCH1 therapies.

RESULTS

Pten loss confers resistance to NOTCH inhibition in T-ALL

To analyze the effects of *Pten* inactivation in the response of primary NOTCH1-induced leukemia cells to GSI therapy *in vivo* we generated a mouse model of NOTCH1 induced T-ALL with conditional and inducible loss of *Pten.* Towards this goal we infected bone marrow hematopoietic progenitors from tamoxifen-inducible conditional *Pten* knockout mice (*Rosa26*$^{Cre\text{-}ERT2/+}$ *Pten*$^{f/f}$) with retroviruses expressing a constitutively active oncogenic mutant form of the NOTCH1 receptor (NOTCH1 L1601P Δ-PEST)[8] and transplanted them into isogenic recipients, which consequently developed NOTCH1-induced T-ALLs. We then injected these NOTCH1-induced *Pten*-conditional tumor cells into secondary recipients and treated them with vehicle only or tamoxifen in order to generate *Pten*-positive (non-deleted) and *Pten*-deleted isogenic tumors, respectively. Treatment of *Pten*-positive leukemia-bearing mice with DBZ, a highly active GSI[9], induced a marked response to therapy by *in vivo* bioimaging (Fig. 1a) and a significant improvement in survival compared with vehicle-only treated controls ($P < 0.005$) (Fig. 1b and Supplementary Fig. 1). In contrast, all mice harboring isogenic *Pten*-deleted tumors showed increased resistance to anti-NOTCH inhibition therapy and progressed under treatment (Fig. 1a,b and Supplementary Fig. 1). Analysis of cell proliferation in T-ALL lymphoblasts isolated from *Pten*-positive and *Pten*-deleted leukemia-bearing mice treated with DBZ showed decreased proliferation upon NOTCH inhibition in *Pten*-positive tumors, a phenotype rescued by genetic loss of *Pten* (Fig. 1c). Importantly, analysis of NOTCH1 signaling showed complete clearance of activated NOTCH1 protein (ICN1) both in *Pten*-positive and *Pten*-deleted tumors treated with DBZ, supporting that *Pten* loss does not impair the uptake or intrinsic activity of this GSI (Fig. 1d). Moreover, Myc, a critical downstream effector of the oncogenic effects of NOTCH1 was effectively downregulated in *Pten*-positive and *Pten*-deleted leukemias treated with DBZ (Fig. 1d and Supplementary Fig. 1), ruling out increased Myc expression secondary to *Pten* loss as a potential mechanism of escape from the antileukemic effects of NOTCH1 inhibition. Next, and to assess the effects of isogenic *PTEN* loss in human cells, we infected a human primary xenograft (PDTALL#19) with lentiviruses expressing a shRNA targeting *PTEN* (shPTEN) or a shRNA control (shLUC), and confirmed the knockdown of *PTEN* levels in cells expressing shPTEN (Supplementary Fig. 2). Expression of the shLUC did not alter the response to GSI (Supplementary Fig. 2). In contrast, and most notably, *PTEN* knockdown restored leukemia cell growth in the context of GSI treatment (Supplementary Fig. 2). Overall, these results show that *Pten* loss and consequent constitutive activation of the PI3K-AKT pathway can confer resistance to anti-NOTCH1 GSI therapy *in vivo*.

To investigate the underlying mechanisms mediating resistance to NOTCH inhibition in *Pten*-null T-ALL tumor cells we performed gene expression profiling of isogenic *Pten*-positive and *Pten*-deleted leukemia lymphoblasts after acute treatment with DBZ *in vivo.* This analysis revealed that, while direct NOTCH1 target genes (such as *Hes1*, *Dtx1, Ptcra, Heyl* and *Notch3*) are effectively downregulated in both *Pten*-positive and *Pten*-deleted tumors (Fig 1e–g and Supplementary Fig. 1), genetic ablation of *Pten* elicits a global reversal of much of the transcriptional effects of NOTCH inhibition (Fig. 1f,h and Supplementary Fig. 1). Functional annotation of genes downregulated by NOTCH inhibition whose expression is restored upon *Pten* loss revealed a marked enrichment in pathways associated with cell anabolism, such as ribosomal RNA processing and amino acid and nucleobase biosynthesis (Fig. 1f and Supplementary Table 1). Conversely, genes selectively upregulated by GSI treatment in *Pten*-positive tumors only are predominantly implicated in apoptosis (e.g. regulation of cell death and caspase regulator activity), autophagy (e.g. lytic vacuole, regulation of autophagy and lysosome) and catabolism (e.g. lipid catabolism, ubiquitin conjugation and phagocytosis)(Fig. 1f and Supplementary Table 1).

Impaired metabolism by NOTCH inhibition in T-ALL

Following up on these results, we decided to explore the metabolic effects of NOTCH inhibition and *Pten* loss by performing a broad-based metabolomic analysis by LC-MS/MS of isogenic *Pten*-positive and *Pten*-deleted NOTCH1-induced leukemia cells treated with the DBZ GSI *in vivo.* These analyses showed that inhibition of NOTCH signaling by DBZ in NOTCH1-induced *Pten*-positive tumors resulted in the accumulation of glucose and proximal (glucose-6-phosphate, fructose-6-phosphate and fructose-1,6-biphosphate) and distal glycolytic intermediates (3-phosphoglycerate and 2,3-diphosphoglycerate) (Fig. 2a), coupled with higher levels of ribose-5-phosphate and ribulose-5-phosphate/xylulose-5-phosphate in the pentose phosphate pathway. Moreover, inhibition of NOTCH signaling was associated with elevated free amino acid levels (Supplementary Fig. 3), potentially linked with increased autophagy; and increased levels of glutamine, but not glutamate (Fig. 2a). Notably, loss of *Pten* resulted in increased lactate levels (Fig. 2a) and reversed the accumulation of glycolytic intermediates induced by NOTCH1 inhibition in *Pten*-positive T-ALL cells (Fig. 2a).

To directly assess the role of impaired carbon metabolism in mediating the antileukemic effects of NOTCH1 inhibition with GSIs, we evaluated the capacity of methyl pyruvate, a membrane soluble metabolite that bypasses glycolysis and can be incorporated directly into the tricarboxylic acid cycle (TCA cycle)[10], to rescue the effects of NOTCH inhibition in DND41, a *NOTCH1*-mutated and PTEN-positive T-ALL cell line[7]. Consistent with previous reports[11], inhibition of NOTCH1 signaling with DBZ induced decreased cell size and proliferation with cell cycle arrest in G1 (Fig. 2b–d). Methyl pyruvate treatment induced a slight increase in cell size, and abrogated the antileukemic effects of NOTCH inhibition on cell growth (10.5% reduction in size by DBZ in vehicle control cells *vs.* 2.6% decrease in cell diameters in DBZ treated cells grown in media supplemented with methyl pyruvate, $P < 0.001$) and proliferation (Fig. 2b–d). Similarly, bypass of glutaminolysis with membrane-soluble dimethyl α-ketoglutarate[12], effectively antagonized the inhibitory effects of NOTCH1 inhibition in cell size (7.7% reduction in size by DBZ in vehicle control cells *vs.* 2.6% decrease in cell diameters in DBZ treated cells grown in media supplemented with dimethyl α-ketoglutarate, $P < 0.001$) and proliferation (Fig. 2e–g), further supporting a major role for inhibition of carbon metabolism as a key effector of the antileukemic effects of NOTCH1 inhibition in T-ALL. We obtained similar results in a second *NOTCH1*-mutated PTEN-positive cell line (HPB-ALL) (Supplementary Fig. 4).

***Pten*-positive T-ALLs rely on autophagy upon NOTCH inhibition**

The transcriptional and metabolic changes associated with NOTCH1 inhibition in *Pten*-positive T-ALL tumor cells are indicative of decreased anabolism and a concomitant increase in catabolic processes. In this context, electron microscopy analysis showed increased autophagy *in vivo* upon DBZ treatment in *Pten*-positive NOTCH-induced leukemias, which was effectively rescued in *Pten*-deleted tumors (Fig. 3a). In addition, western blot analyses showed increased levels of the LC3a II autophagic marker in *Pten*-positive leukemias treated with DBZ, whereas *Pten* loss efficiently rescued this phenotype (Fig. 3b and Supplementary Fig. 5). Based on these observations we hypothesized that induction of autophagy can contribute to sustain cell survival during NOTCH1 inhibition by recycling essential metabolites required for leukemia cell metabolism. To test this model, we generated NOTCH1-induced T-ALLs from tamoxifen-inducible conditional *Atg7* knockout ($Rosa26^{Cre\text{-}ERT2/+}$ $Atg7^{f/f}$)[13] hematopoietic progenitors, which were subsequently treated with vehicle only or tamoxifen in order to generate *Atg7*-positive (non-deleted) and *Atg7*-deleted isogenic tumors, respectively (Fig. 3c). Treatment of NOTCH1-induced *Atg7*-positive leukemia-bearing mice with DBZ induced a marked *in vivo* antileukemic response and significantly improved survival ($P < 0.005$) (Fig. 3d), which was markedly increased after abrogation of autophagy via tamoxifen-induced deletion of *Atg7* ($P < 0.005$) (Fig. 3d).

Overall, these results support that inhibition of NOTCH1 signaling drives a metabolic crisis in *Pten*-positive T-ALL tumor cells, rendering leukemia lymphoblasts dependent on autophagy for growth and survival.

NOTCH-induced glutaminolysis is a key carbon source in T-ALL

Next, and to further explore the anabolic effects of NOTCH inhibition and *Pten* deletion in glycolysis and glutaminolysis we performed metabolic tracing studies with ^{13}C isotope-labeled glucose (U-$^{13}C_6$) and glutamine (U-$^{13}C_5$). These studies revealed that NOTCH1-induced leukemias made prominent use of glutamine as a source of carbon. Thus, glutamine-derived ^{13}C was readily converted to glutamate and effectively incorporated into all TCA cycle intermediates (~80% labeling), supporting a major role for glutaminolysis as a carbon source in the metabolism of NOTCH1-induced leukemia (Fig. 4a,b). Glucose labeled the lactate pool (~80% labeling) and contributed to 40–60% of the TCA cycle intermediates citrate, fumarate and malate (Fig. 4a,b). Notably, *Pten* deletion resulted in increased lactate production suggestive of increased glycolysis (Fig. 4c). Moreover, kinetic profiling analysis of glucose and glutamine-derived ^{13}C incorporation into the TCA cycle showed that NOTCH1 inhibition with DBZ decreased the fractional contribution of glucose to lactate, but not to TCA cycle intermediates (Fig. 4d). In contrast, DBZ treatment decreased glutamine labeling of glutamate and TCA cycle intermediates (Fig. 4e). Importantly, the block in glycolysis observed in NOTCH1-induced *Pten*-positive leukemia lymphoblasts treated with DBZ was decreased by isogenic deletion of *Pten* (Fig. 4d). In addition, *Pten* loss reduced the DBZ-induced block in glutamine to glutamate conversion but had no clear effects in the incorporation of glutamine derived carbon to the TCA cycle (Fig. 4e).

Next, we investigated the expression levels of Pten, p-AKT and glutaminase (Gls) in *Pten* wild-type NOTCH1-induced leukemias at the time of disease progression after the four cycles of treatment with DBZ. Notably, these leukemic cells show decreased levels of Pten, with a concomitant increase in p-AKT levels, as well as increased Gls (Fig. 5a). These results suggest that T-ALL lymphoblasts treated with GSI might be overcoming the therapeutic effects of NOTCH1 inhibition by downregulating Pten and upregulating Gls expression *in vivo*.

Following on these results we further explored the mechanisms downstream of NOTCH1 and PTEN in the control of leukemia cell growth. Expression of critical signaling factors controlled by NOTCH1 and downregulated by GSI treatment in both *Pten*-positive and *Pten*-deleted T-ALL cells such as IL7R and Ptcra had no effect on the response of *Pten*-positive cells to either vehicle or GSI therapy (Fig. 5b–g and Supplementary Fig. 6). In contrast, mice transplanted with *Pten*-positive T-ALL tumor cells infected with constitutively active AKT (myristoylated-AKT) reversed the anabolic (downregulated) and catabolic (upregulated) transcriptional changes associated with NOTCH1 inhibition (Supplementary Fig. 7), as well as the glycolytic block, the block in glutaminolysis and the increase in free amino acids observed by LC-MS/MS (Supplementary Fig. 8), and induced overt resistance to NOTCH1 inhibition and progression under treatment (Fig. 5b). In addition, analysis of metabolic regulators showed that expression of GLS significantly restored leukemia cell growth in the context of inhibition of NOTCH1 signaling (Fig. 5c).

Similarly, expression of PKM2, a cancer associated isoform of the glycolytic enzyme pyruvate kinase resulted in enhanced leukemia cell growth in the context of inhibition of NOTCH1 signaling (Fig. 5d). In contrast, expression of 3-Phosphoglycerate dehydrogenase (PHGDH), the first and rate-limiting step in the phosphorylated pathway of serine biosynthesis also associated with tumor cell growth[14], had limited or no effect in the response of tumor cells to NOTCH1 inhibition with DBZ (Fig. 5e). Cells overexpressing GLS increase their glutamine utilization (Supplementary Fig. 9) but still show downregulation of glutaminolysis upon DBZ treatment in glutamine-derived ^{13}C kinetic labeling analyses (Supplementary Fig. 9), suggesting that increased GLS expression may confer resistance to DBZ treatment in this experiment by sheer mass effect. Overall, these results demonstrate that metabolic manipulation can modify the *in vivo* response to GSI treatment in NOTCH1-induced leukemias.

Therapeutic targeting of NOTCH1 and glutaminase in T-ALL

The identification of glutaminolysis as a critical effector of the antileukemic response to NOTCH1 inhibition in T-ALL supports that pharmacologic inhibition of glutaminase may impair leukemic cell growth and sensitize T-ALL cells to NOTCH1 inhibition therapies. To test this hypothesis, we analyzed the effects of glutaminase inhibition on leukemia cell growth and survival. Treatment of HPB-ALL and DND41 T-ALL cells with BPTES, a potent and specific glutaminase inhibitor[15], impaired leukemia cell growth (Fig. 6a and Supplementary Fig. 10), and showed strong and significantly synergistic antileukemic effects in combination with NOTCH1 inhibition with DBZ (Combination Index at ED50 = 0.012 in HPB-ALL and 0.666 in DND-41 cells) (Fig. 6b and Supplementary Fig. 10). Notably, this phenotype was primarily driven by increased cytotoxicity in cells treated with BPTES and DBZ in combination (Fig. 6c,d and Supplementary Fig. 10). In contrast, treatment with 2-deoxyglucose, a non-metabolizable glucose analog that inhibits glycolysis[16], showed additive antileukemic effects in combination with DBZ, further supporting a dominant role for glutaminolysis over glycolysis downstream of NOTCH1 signaling in T-ALL (Supplementary Fig. 11). Importantly, Crispr-Cas9-mediated *PTEN* inactivation in the HPB-ALL cell line conferred resistance to treatment with DBZ alone and in combination with BPTES, further supporting a role for *PTEN* loss as driver of resistance to GSI therapy in human cells (Supplementary Figure 12). To further explore the clinical relevance of glutaminase inhibition therapies in combination with GSIs we next tested the efficacy of the NOTCH1 inhibition with DBZ, glutaminase inhibition with BPTES and the combination of DBZ plus BPTES compared to vehicle only (DMSO) treatment in mice xenografted with two independent *NOTCH1*-mutant (PDTALL#10: *NOTCH1* L1601P, R1609H; PDTALL#19: *NOTCH1* P1606LV, V2412fs) and *PTEN* wild type human-derived primary T-ALL xenografts. In this experiment, mice treated with BPTES showed progressive tumor growth *in vivo* similar to that observed in vehicle-treated controls, while NOTCH inhibition with DBZ induced significant antitumor responses (Fig. 6e,f), which were markedly and significantly increased by glutaminase inhibition in the DBZ plus BPTES treatment group (Fig. 6e,f).

Next, and to better assess the interaction between NOTCH signaling and *Pten* loss in the response to anti-NOTCH1 and glutaminase inhibition therapies, we analyzed the effects of vehicle only (DMSO), BPTES, DBZ and BPTES plus DBZ in mice transplanted with our NOTCH1-induced *Pten*-positive or NOTCH1-induced *Pten*-deleted mouse isogenic tumor cells. In this experiment, inhibition of glutaminolysis significantly increased the antileukemic effects of NOTCH1 inhibition in NOTCH1-induced *Pten*-positive T-ALL bearing animals treated with DBZ plus BPTES (Fig. 6g and Supplementary Fig. 13), which translated into increased survival (Supplementary Fig. 14). In contrast, and most notably, *Pten*-deleted T-ALL cells showed not only impaired response to GSI therapy, but also to treatment with DBZ plus BPTES in combination (Fig. 6h). These results are consistent with our metabolic studies showing that *Pten* loss induces a hyperglycolytic phenotype, which would render T-ALL cells not only resistant to NOTCH inhibition, but also less sensitive to inhibition of glutaminolysis as result of increased glucose derived carbon input to the TCA cycle.

Finally, to genetically test the interaction between NOTCH signaling and glutaminase *in vivo* and rule out a potential off-target effect of BPTES, we generated NOTCH1-induced T-ALLs from tamoxifen-inducible conditional *Gls* knockout ($Rosa26^{Cre\text{-}ERT2/+}$ $Gls^{f/f}$) hematopoietic progenitors, which were subsequently transplanted into secondary recipients and treated with vehicle only or tamoxifen in order to generate *Gls*-positive (non-deleted) and *Gls*-deleted isogenic tumors, respectively (Fig. 6i). Treatment of NOTCH1-induced *Gls*-positive leukemia-bearing mice with DBZ induced a marked *in vivo* antileukemic response and significantly improved survival ($P < 0.005$) (Fig. 6j). In addition, tamoxifen-induced deletion of glutaminase resulted in overt anti-leukemic effects, which were markedly and significantly enhanced ($P < 0.005$; 40% complete remission) upon GSI treatment (Fig. 6j). This finding fully validates our pharmacological results and highlights glutaminolysis as a key player and therapeutic target in NOTCH1-induced T-ALL.

DISCUSSION

Co-occurring activating mutations in *NOTCH1* and mutations and deletions in *PTEN* are characteristic of GSI-resistant T-ALL cell lines[7] and can also be found in primary patient samples[7,17]. However, *PTEN* mutant leukemias may be still at least partially responsive to NOTCH1 inhibition[18] and epigenetic reprogramming of NOTCH1-driven T-ALL cell lines has been recently implicated in tumor escape from anti-NOTCH1 therapies after prolonged *in vitro* treatment with GSIs[19], supporting that additional genetic and epigenetic factors may coordinately contribute to drive resistance to GSI based anti-NOTCH1 therapies. To formally address the specific role of *Pten* inactivation as driver of resistance to GSI therapy we engineered a model of NOTCH1 induced leukemia with conditional inducible loss of *Pten*, which allowed the direct comparison of *Pten*-positive and *Pten*-deleted isogenic tumors in immune-competent isogenic secondary recipients *in vivo*. In this model, NOTCH1-induced leukemias showed effective but variable antileukemic responses to GSI therapy even in the context of tumors generated with the same activated NOTCH1 allele. These results substantiate the value of our analyses across heterogeneous tumors with different levels of primary NOTCH1 oncogene addiction. Most notably, although *Pten* deletion did not render the cells completely insensitive to NOTCH inhibition with GSI, in each case mutational loss of *Pten* effectively impaired the response to NOTCH1 inhibition therapy and all mice harboring *Pten*-deleted leukemias showed overt progression under therapy, a hallmark criteria of therapy resistance in the clinic, with 100% mortality by the end of the fourth cycle of treatment. Similarly, PTEN knockdown in a primary human T-ALL xenograft also impaired the therapeutic efficacy of GSI treatment. These results conclusively demonstrate that mutational loss of *Pten* can induce resistance to GSI therapy in primary tumor cells *in vivo*.

Mechanistically, gene expression profiling analyses revealed that inhibition of the γ-secretase complex effectively suppressed NOTCH1 activation and that key genes controlled by NOTCH1 were effectively downregulated in both *Pten*-wild type and *Pten*-deleted tumors. In addition pathway analysis of gene expression programs controlled by NOTCH1 in *Pten*-wild type and *Pten*-deleted T-ALL tumor cells revealed a dominant effect NOTCH1 inhibition in the suppression of anabolic routes with concomitant upregulation of catabolic genes. The broad transcriptional effects of NOTCH1 inhibition across different metabolic pathways are reminiscent of those induced by *Kras*^{G12D} inactivation in pancreatic ductal adenocarcinoma tumor cells[20] and support that the antileukemic effects of NOTCH1 inhibition in T-ALL may be mediated at least in part by inhibition of cell metabolism. Notably, this model is consistent with the decreased cell growth and cell size phenotypes typically induced by NOTCH1 inhibition in *PTEN* wild type GSI-sensitive human T-ALL cell lines[5,7]. Unexpectedly, outside NOTCH1 direct target genes, *Pten* deletion had profound effects in the transcriptional response of NOTCH1-induced leukemias to anti-NOTCH1 therapy and induced effective reversal of GSI-induced anabolic gene downregulation and abrogation of the catabolic signature associated with NOTCH1 inhibition in *Pten*-wild type tumors. These results support a significant transcriptional input of the PI3K-AKT signaling pathway in the control of cell metabolism that is antagonistic to that of suppression of oncogenic NOTCH1 in T-ALL. Consistently, we observed increased autophagy in *Pten*-wild type tumors, but not in *Pten*-deleted leukemias upon NOTCH1 inhibition. Activation of autophagy upon GSI treatment and increased GSI antileukemic effects in autophagy-deficient *Atg7* null tumors support that NOTCH1 inhibition forces tumor cells to resource to this catabolic mechanism to obtain critical metabolic intermediates for sustained cell growth in *Pten*-wild type T-ALLs[21].

Integration of these results with global metabolic profiling and metabolic isotope tracing analyses revealed a negative effect of NOTCH1 inhibition in glycolysis and glutaminolysis in *Pten*-wild type leukemias. Notably, genetic loss of *Pten* or activated AKT expression resulted in increased intracellular lactate levels supporting increased glycolytic efficiency in *Pten*-deleted tumors, a finding consistent with the well-established role of the PI3K-AKT pathway in inducing aerobic glycolysis[10,22–25]. Moreover, and perhaps most surprisingly, metabolic isotope labeling analyses unveiled a most prominent role for glutaminolysis in feeding carbon into the TCA cycle. Consistently, glutaminase inhibition or genetic deletion of glutaminase were highly synergistic with GSI treatment and induced marked therapeutic responses *in vivo*. Notably, the therapeutic response to combined NOTCH and glutaminase inhibition is also abrogated by loss of *Pten*. This is not surprising since the switch to a hypergycolytic phenotype induced by *Pten* loss would make T-ALL cells less dependent on glutaminolysis because of increased glucose derived carbon input to the TCA cycle.

Overall, our results highlight the fundamental importance of NOTCH1 signaling in the control of leukemia cell metabolism, extend our understanding of the prominent role of PTEN and the PI3K pathway in the control of oncogenic cell growth and provide the basis for the design of new therapeutic strategies targeting cell metabolism for the treatment of T-ALL.

ONLINE METHODS

Mice and animal procedures

We maintained all animals in specific pathogen-free facilities at the Irving Cancer Research Center at Columbia University Medical Campus. The Columbia University Institutional Animal Care and Use Committee (IACUC) approved all animal procedures. *Rosa26*$^{Cre\text{-}ERT2/+}$mice expressing a tamoxifen-inducible form of the Cre recombinase from the ubiquitous *Rosa26* locus[26], *Pten* conditional knockout (*Pten*^{fl})[27] and *Atg7* conditional knockout (*Atg7*^{fl})[13] mice have been previously described. To generate NOTCH1-induced T-ALL tumors in mice, we performed retroviral transduction of bone marrow cells enriched in Lineage negative cells (using Miltenyi kit #130-090-858, following manufacturer's guidelines) with activated forms of the NOTCH1 oncogene (NOTCH1 L1601P ΔPEST in *Pten*^{fl} cells or ΔE-NOTCH1 in *Atg7*^{fl} and *Gls*^{fl} cells) and transplanted them via intravenous injection into lethally irradiated recipients as previously described[8].

For all subsequent studies, we bought secondary recipient C57BL6 females (6–8 week old) from Taconic Farms. Animals were randomly assigned to the different treatment groups and no blinding was done. For survival studies, we transplanted leukemia cells from primary recipients into secondary recipients sub-lethally irradiated (4 Gy); two days after the transplant, we treated the mice tamoxifen (5mg per mouse by intra-peritoneal injection) to induce deletion of either the *Pten,* the *Atg7* or the *Gls* locus, or with vehicle only (Corn oil) for the control groups; 4 days later, we subdivided the mice in groups treated with vehicle only (2.3% DMSO in 0.00.5% Methylcellulose, 0.1% Tween-80) or with DBZ (5 mg kg^{-1}) on a 4 days-on and 3 days-off basis.

For acute treatment analyses, we transplanted leukemia cells from primary recipients into secondary recipients, which were treated with vehicle or tamoxifen (to induce *Pten* deletion), as described before. We monitored the mice until they showed more than 70% of GFP positive cells in peripheral blood and then, mice were treated twice, 16 hours apart, with vehicle only or DBZ (5 mg kg^{-1}). 4 hours after the second treatment, mice were sacrificed and splenic samples were collected and subsequently analyzed (^{13}C-labeling) or snap-frozen for further analyses (microarrays, RT-PCR, Western Blots, metabolomics).

For the cherry rescue experiment *in vivo*, we infected leukemia cells from the mouse tumors previously generated with retroviral particles expressing the red cherry fluorescent protein (MSCV empty-mCherry) or a fusion protein of the red cherry fluorescent protein together with either IL7R (MSCV IL7R-IRES-mCherry), preTCR-alpha (MSCV Ptcra-IRES-mCherry), myristoylated-AKT (MSCV Myr-AKT-IRES-mCherry), Glutaminase (MSCV GLS-IRES-mCherry), PKM2 (MSCV PKM2-IRES-mCherry) or PHGDH (MSCV PHGDH-IRES-mCherry) and re-injected them in sub-lethally irradiated C57/BL6 mice (4 Gy).

For drug synergism studies *in vivo*, we infected leukemia cells from the mouse tumors previously generated with retroviral particles expressing a fusion protein between the red cherry fluorescent protein and luciferase (MigR1 mCherryLuc) and re-injected them in sub-lethally irradiated C57/BL6 mice (4 Gy). For the human primary leukemia xenograft experiment, we infected PDTALL#19 and PDTALL#10 cells with lentiviral particles expressing the red cherry fluorescent protein and luciferase (FUW-mCherry-Luc) and re-injected them in NRG mice (6 – 8 week old, both males and females). We analyzed the efficacy of glutaminase inhibition with BPTES in combination with DBZ in secondary NRG recipient mice transplanted with these mCherry-Luciferase expressing cells. In these experiments, we treated the mice with daily intraperitoneal doses of vehicle (DMSO), BPTES (25 mg kg^{-1}), DBZ (5 mg kg^{-1}) or BPTES (25 mg kg^{-1}) plus DBZ (5 mg kg^{-1}) for 6 days. We evaluated disease progression and therapy response by *in vivo* bioimaging with the In Vivo Imaging System (IVIS, Xenogen).

Microarray gene expression profiling

We isolated RNA from leukemic cells from spleen samples collected from mice acutely treated with Vehicle or DBZ using RNeasy plus mini kit (Qiagen) according to manufacturer's protocol. RNA (1 μg) from *Pten*-positive and *Pten*-deleted leukemic cells treated with vehicle or DBZ was amplified and labeled using 3′ IVT Express Kit (Affymetrix) and hybridized on GeneChip Mouse Genome 430 2.0 Arrays (Affymetrix) according to the manufacturer's protocol. RNA (1 μg) from *Pten*-positive mCherry and *Pten*-positive myr-AKT leukemic cells treated with vehicle or DBZ was amplified and labeled with the Illumina TotalprepRNA kit and hybridized on Illumina MouseWG-6 v2.0 BeadChip arrays according to the manufacturer's protocol. For the Affymetrix arrays, we performed inter-array normalization with the GC-RMA algorithm using open-source Bioconductor software[28]. For the Illumina arrays, expression values were log2 transformed and quantile normalized. We evaluated group differences using t-test and fold change.

For the Pathway Enrichment analyses, gene sets of interest, including differentially expressed genes by GSI that were rescued by *Pten* deletion, were tested for functional annotations enrichment using the web-based DAVID bioinformatics tools available at http://david.abcc.ncifcrf.gov.

We compared the enrichment of genes differentially expressed by GSI in *Pten*-positive and *Pten*-deleted tumors with the genes differentially expressed by GSI in *Pten*-positive mCherry expressing and in *Pten*-positive mCherry-myrAKT expressing leukemias by GSEA[29] using the t-test metric and 10,000 permutations of the gene list.

Metabolomic analyses

We analyzed leukemic spleen samples from mice acutely treated with Vehicle or DBZ by GC/MS and LC/MS/MS. Briefly, we collected splenic samples and snap froze them 4 hours after the second round of *in vivo* treatment with Vehicle or DBZ. We then extracted the samples and prepared them for analysis using standard solvent extraction methods. The extracted samples were split into equal parts for analysis on the GC/MS and LC/MS/MS platforms in Metabolon facilities.

Dataset comprises a total 267 named biochemicals. Following log transformation and imputation with minimum observed values for each compound, we used ANOVA contrasts for pairwise comparisons to identify biochemicals that differed significantly between experimental groups. Analysis by two-way ANOVA identified biochemicals exhibiting significant interaction and main effects for experimental parameters of *Pten* expression and DBZ treatment. We calculated an estimate of the false discovery rate (q-value) to take into account the multiple comparisons that normally occur in metabolomic-based studies. For example, when analyzing 200 compounds, we would expect to see about 10 compounds meeting the $p \leq 0.05$ cut-off by random chance.

^{13}C labeling studies

We cultured leukemia cells collected from the spleens of acutely treated mice (as described before) in RPMI media supplemented with 10% dialyzed fetal bovine serum and 10 mM ^{13}C-Glucose or 4 mM ^{13}C-Glutamine (Cambridge Isotope Laboratories). Cells were cultured for 6 hours for the steady-state glucose and glutamine experiments and for 30 minutes, 1 hour, 2 hours and 6 hours for the glucose and glutamine kinetics experiment. After labeling, we rinsed the cells in ice-cold normal saline and lysed them with three freeze-thaw cycles in cold 50% methanol. The lysates were centrifuged to remove precipitated protein, a standard (50 nmols of sodium 2-oxobutyrate) was added, and the samples were evaporated and derivatized by trimethylsilylation (Tri-Sil HTP reagent, Thermo Scientific). We then injected three microliters of the derivatized material onto an Agilent 6970 gas chromatograph equipped with a fused silica capillary GC column (30 m length, 0.25 mm diameter) and networked to an Agilent 5973 mass selective detector. Retention times of all metabolites of interest were validated using pure standards. The measured distribution of mass isotopomers was corrected for natural abundance of ^{13}C.

Extracellular lactate was measured in 100ul of media from cells that had been cultured for 6 hrs in media made with dialyzed serum. Removal of lipids and proteins from the media was accomplished with a 1:1:1 chloroform:methanol:water extraction. Prior to evaporation, a uniformly labeled ^{13}C lactate standard (Cambridge) was added to the aqueous phase. After being dried, the sample was derivatized with 100ul of Tri-Sil (Thermo Scientific) for 10min at 75C then 10min at room temperature. 5ul of the derivatized sample was injected onto an Agilent 6890 GC networked to an Agilent 5975 Mass Selective Detector. The comparison of the labeled lactate standard to the unlabeled lactate pool derived from cellular metabolism allowed for the quantitation of lactate abundance in the sample. We measured ammonia with a spectrophotometric assay (Megazyme).

Quantitative real time PCR

We generated cDNA with the ThermoScript RT-PCR system (Invitrogen) and analyzed it by quantitative real-time PCR (FastStart Universal SYBR Green Master Mix (Roche) using a 7300 Real-Time PCR System (Applied Biosystems). Relative expression levels were based on *Gapdh* as a reference control.

Western Blotting

We performed Western blots using standard procedures. Antibodies against Cleaved Notch1 (#4147), GAPDH (#5174), LC3a (#4599), p(S473)AKT (#9271), p(T308)AKT (#9275), AKT total (#9272) and PTEN (#9188) were from Cell Signaling technologies (1:1000 dilution). Glutaminase antibody was from proteintech (1:1000, #20170-1-AP) or a purified rabbit polyclonal antibody against GLS[30] (1:1000 dilution). ATG7 antibody was from Sigma-Aldrich (1:1000, #A2856). Myc antibody (1:200, N-262) was obtained from Santa Cruz. GFP antibody (1:1000, #11814460001) was obtained from Roche.

Inhibitors and drugs

DBZ ((S)-2-(2-(3,5-Difluorophenyl)acetamido)-N-((S)-5-methyl-6-oxo-6,7-dihydro-5H-dibenzo[b,d]azepin-7-yl)propanamide) was obtained from Syncom (#SIC-020042). BPTES (Bis-2-(5-phenylacetamido-1,3,4-thiadiazol-2-yl)ethyl sulfide; #SML0601), 2-deoxyglucose (#D6134), tamoxifen (#T5648), dimethyl ketoglutarate (#349631) and methyl pyruvate (#371173) were obtained from Sigma-Aldrich.

Cell lines

(HEK) 293T (purchased from ATCC), HPB-ALL and DND41 (obtained from DSMZ) cell lines were cultured in standard conditions in RPMI media supplemented with 10% FBS and 1% Penicillin/Streptomycin. Cell lines were regularly authenticated and tested for mycoplasma. To CRISPR-out *PTEN* in HPB-ALL cells, we designed a gRNA against *PTEN* using the E-CRISP software (http://www.e-crisp.org/E-CRISP/designcrispr.html). This gRNA was subsequently cloned into pL-CRISPR.EFS.GFP vector (Addgene plasmid #57818)[31]. We then infected HPB-ALL cells with this construct and the GFP positive population was sorted and further analyzed.

Human primary xenografts

T-ALL samples were provided by Columbia Presbyterian Hospital and University of Padova with informed consent and analyzed under the supervision of the Columbia University Medical Center Institutional Review Board committee.

Cell viability, cell size and flow cytometric analysis

We analyzed cell line viability upon treatment with BPTES (10 μM) and DBZ (250 nM) alone and in combination using the Cell Proliferation Kit I (Roche). We analyzed apoptosis by flow cytometry with APC AnnexinV Apoptosis Kit I (BD Biosciences). We used Propidium Iodide (Sigma) DNA staining to analyze cell cycle distribution.

For the metabolic rescue experiment, cells were maintained on RPMI buffered with 40 mM HEPES, and treated with methyl pyruvate (10 mM) or dimethyl ketoglutarate (8 mM) and/or DBZ (250 nM). We added new media every two days.

For the measurement of PTEN intracellular levels in PDTALL 19 human primary xenografted samples, we removed red cells from peripheral blood samples by incubation with red blood cell lysis buffer (155 mM NH4Cl, 12 mM KHCO3 and 0.1 mM EDTA) for 5 min at room temperature. We then stained the samples with anti-human-CD45 (eBioscience, Cat# 17-0459-42, clone HI30, dilution 1:200). Next, we performed fixation/permeabilization using Foxp3/Transcription Factor Staining Buffer Set (eBioscience Cat# 00-5523), following manufacturer's instructions. Finally, we performed intracellular staining with anti-PTEN-PE (BD Phosflow, Cat# 560002, clone A2B1, dilution 1:5) and we used PE-labeled mouse IgG1 isotype as a control (BD Pharmingen, Cat# 551436, dilution 1:5).

Statistical analyses

We performed statistical analysis by Student's *t*-test. We considered results with $P < 0.05$ as statistically significant. We analyzed drug synergism using the median-effect method of Choy and Talay[32] and used the CalcuSyn software (Biosoft, Great Shelford, Cambridge, UK) to calculate the combination index (CI) and perform isobologram analysis of drug interactions. Survival in mouse experiments was represented with Kaplan-Meier curves and significance was estimated with the log-rank test (Prism GraphPad).

Supplementary Material

Refer to Web version on PubMed Central for supplementary material.

Acknowledgments

This work was supported by the US National Institutes of Health (grants R01CA129382 and CA120196 to A.A.F.), the Stand Up To Cancer Innovative Research Award (A.A.F.) and the Swim Across America Foundation (A.A.F). J.M. and J.M.M. were supported by CVI-6656. We are grateful to J. Aster (Department of Pathology, Brigham and Women's Hospital, Harvard Medical School, Boston, MA, USA) for the MigR1-*NOTCH1* L1601P ΔPEST vector, P. P. Pandolfi (Cancer Research Institute, Beth Israel Deaconess Cancer Center, Department of Medicine and Pathology, Beth Israel Deaconess Medical Center, Harvard Medical School, Boston, MA, USA) for the $Pten^{fl}$ conditional knockout mouse, T. Ludwig (Institute for Cancer Genetics, Columbia University Medical Center, New York, NY, USA) for the $Rosa26^{Cre\text{-}ERT2/+}$ mouse, M. Komatsu (Tokyo Metropolitan Institute of Medical Science, Setagaya-ku, Tokyo, Japan) for the $Atg7^{fl}$ mouse, S. Indraccolo (UOC Immunologia e Diagnostica Molecolare Oncologica, Istituto Oncologico Veneto — Istituto di Ricovero e Cura a Carattere Scientifico, Padova, Italy) for xenograft T-ALL cells and R. Baer and C. Lopez-Otin for helpful discussions and revision of the manuscript. D.H. is a Leukemia and Lymphoma Society postdoctoral fellow. M.S-M. and A.A.W. are postdoctoral fellows supported by the Rally Foundation. L.B. is a Lymphoma Research Foundation postdoctoral fellow.

REFERENCES FOR MAIN TEXT

1. Hori K, Sen A, Artavanis-Tsakonas S. Notch signaling at a glance. Journal of cell science. 2013; 126:2135–2140. [PubMed: 23729744]
2. Rothenberg EV, Moore JE, Yui MA. Launching the T-cell-lineage developmental programme. Nat Rev Immunol. 2008; 8:9–21. [PubMed: 18097446]
3. Thompson PK, Zuniga-Pflucker JC. On becoming a T cell, a convergence of factors kick it up a Notch along the way. Semin Immunol. 2011; 23:350–359. [PubMed: 21981947]
4. Ciofani M, Zuniga-Pflucker JC. Notch promotes survival of pre-T cells at the beta-selection checkpoint by regulating cellular metabolism. Nature immunology. 2005; 6:881–888. [PubMed: 16056227]
5. Weng AP, et al. Activating mutations of NOTCH1 in human T cell acute lymphoblastic leukemia. Science. 2004; 306:269–271. [PubMed: 15472075]
6. Selkoe D, Kopan R. Notch and presenilin: Regulated intramembrane proteolysis links development and degeneration. Annu Rev Neurosci. 2003; 26:565–597. [PubMed: 12730322]
7. Palomero T, et al. Mutational loss of PTEN induces resistance to NOTCH1 inhibition in T-cell leukemia. Nature medicine. 2007; 13:1203–1210.

8. Chiang MY, et al. Leukemia-associated NOTCH1 alleles are weak tumor initiators but accelerate K-ras-initiated leukemia. The Journal of clinical investigation. 2008; 118:3181–3194. [PubMed: 18677410]

9. Milano J, et al. Modulation of notch processing by gamma-secretase inhibitors causes intestinal goblet cell metaplasia and induction of genes known to specify gut secretory lineage differentiation. Toxicological sciences : an official journal of the Society of Toxicology. 2004; 82:341–358. [PubMed: 15319485]

10. Buzzai M, et al. The glucose dependence of Akt-transformed cells can be reversed by pharmacologic activation of fatty acid beta-oxidation. Oncogene. 2005; 24:4165–4173. [PubMed: 15806154]

11. Palomero T, et al. NOTCH1 directly regulates c-MYC and activates a feed-forward-loop transcriptional network promoting leukemic cell growth. Proceedings of the National Academy of Sciences of the United States of America. 2006; 103:18261–18266. [PubMed: 17114293]

12. Wise DR, et al. Myc regulates a transcriptional program that stimulates mitochondrial glutaminolysis and leads to glutamine addiction. Proceedings of the National Academy of Sciences of the United States of America. 2008; 105:18782–18787. [PubMed: 19033189]

13. Komatsu M, et al. Impairment of starvation-induced and constitutive autophagy in Atg7-deficient mice. The Journal of cell biology. 2005; 169:425–434. [PubMed: 15866887]

14. Locasale JW, et al. Phosphoglycerate dehydrogenase diverts glycolytic flux and contributes to oncogenesis. Nature genetics. 2011; 43:869–874. [PubMed: 21804546]

15. Robinson MM, et al. Novel mechanism of inhibition of rat kidney-type glutaminase by bis-2-(5-phenylacetamido-1,2,4-thiadiazol-2-yl)ethyl sulfide (BPTES). The Biochemical journal. 2007; 406:407–414. [PubMed: 17581113]

16. Tennant DA, Duran RV, Gottlieb E. Targeting metabolic transformation for cancer therapy. Nature reviews Cancer. 2010; 10:267–277. [PubMed: 20300106]

17. Homminga I, et al. Characterization of a pediatric T-cell acute lymphoblastic leukemia patient with simultaneous LYL1 and LMO2 rearrangements. Haematologica. 2012; 97:258–261. [PubMed: 22058201]

18. Medyouf H, et al. Acute T-cell leukemias remain dependent on Notch signaling despite PTEN and INK4A/ARF loss. Blood. 2010; 115:1175–1184. [PubMed: 20008304]

19. Knoechel B, et al. An epigenetic mechanism of resistance to targeted therapy in T cell acute lymphoblastic leukemia. Nature genetics. 2014; 46:364–370. [PubMed: 24584072]

20. Ying H, et al. Oncogenic Kras maintains pancreatic tumors through regulation of anabolic glucose metabolism. Cell. 2012; 149:656–670. [PubMed: 22541435]

21. Zhou S, et al. Autophagy in tumorigenesis and cancer therapy: Dr. Jekyll or Mr. Hyde? Cancer letters. 2012; 323:115–127. [PubMed: 22542808]

22. Elstrom RL, et al. Akt stimulates aerobic glycolysis in cancer cells. Cancer research. 2004; 64:3892–3899. [PubMed: 15172999]

23. Bauer DE, Hatzivassiliou G, Zhao F, Andreadis C, Thompson CB. ATP citrate lyase is an important component of cell growth and transformation. Oncogene. 2005; 24:6314–6322. [PubMed: 16007201]

24. Hatzivassiliou G, et al. ATP citrate lyase inhibition can suppress tumor cell growth. Cancer cell. 2005; 8:311–321. [PubMed: 16226706]

25. Tong X, Zhao F, Thompson CB. The molecular determinants of de novo nucleotide biosynthesis in cancer cells. Current opinion in genetics & development. 2009; 19:32–37. [PubMed: 19201187]

26. Guo K, et al. Disruption of peripheral leptin signaling in mice results in hyperleptinemia without associated metabolic abnormalities. Endocrinology. 2007; 148:3987–3997. [PubMed: 17495001]

27. Trotman LC, et al. Pten dose dictates cancer progression in the prostate. PLoS biology. 2003; 1:E59. [PubMed: 14691534]

28. Gentleman RC, et al. Bioconductor: open software development for computational biology and bioinformatics. Genome biology. 2004; 5:R80. [PubMed: 15461798]

29. Subramanian A, et al. Gene set enrichment analysis: a knowledge-based approach for interpreting genome-wide expression profiles. Proceedings of the National Academy of Sciences of the United States of America. 2005; 102:15545–15550. [PubMed: 16199517]

30. Campos-Sandoval JA, et al. Expression of functional human glutaminase in baculovirus system: affinity purification, kinetic and molecular characterization. The international journal of biochemistry & cell biology. 2007; 39:765–773. [PubMed: 17267261]

31. Heckl D, et al. Generation of mouse models of myeloid malignancy with combinatorial genetic lesions using CRISPR-Cas9 genome editing. Nature biotechnology. 2014; 32:941–946.

32. Chou TC. Drug combination studies and their synergy quantification using the Chou-Talalay method. Cancer research. 2010; 70:440–446. [PubMed: 20068163]

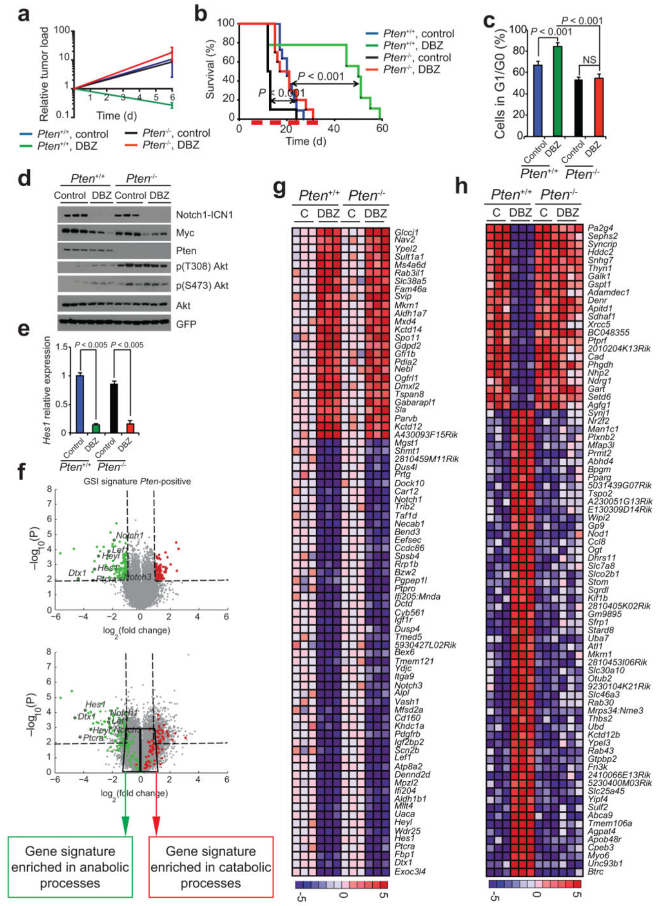

Figure 1. *Pten* loss induces resistance to GSI treatment *in vivo*

(**a**) Changes in tumor load by bioimaging in mice allografted with NOTCH1-induced *Pten*-positive or *Pten*-deleted isogenic leukemias treated with vehicle or DBZ (n = 2 per group). (**b**) Kaplan-Meier survival curve of mice harboring *Pten*-positive and *Pten*-deleted isogenic leukemias treated with 4 cycles of vehicle or DBZ (5 mg Kg^{-1}) on a 4 days ON (red blocks) and 3 days OFF schedule (*Pten*$^{+/+}$/DMSO, n = 11; *Pten*$^{+/+}$/DBZ, n = 9; *Pten*$^{-/-}$/DMSO and *Pten*$^{-/-}$/DBZ, n = 10) (**c**) Cell cycle analyses of leukemias acutely treated with vehicle or DBZ. (**d**) Western blot analyses of intracellular activated NOTCH1, Myc, Akt and Pten expression in leukemias acutely treated with vehicle or DBZ. (**e**) Relative mRNA expression of the NOTCH1 target *Hes1* in leukemias acutely treated with vehicle or DBZ. (**f**) Volcano plot representations of gene expression changes induced by GSI treatment in *Pten*-positive and *Pten*-deleted leukemias. Downregulated or upregulated genes by DBZ in *Pten*-positive cells are marked in green or red, respectively. Dashed boxes indicate differentially expressed genes. Solid line boxes contain non-significantly differentially expressed genes. (**g**) Heat map representation of the top differentially expressed genes upon DBZ treatment in *Pten*-positive and *Pten*-deleted leukemias. (**h**) Heat map representation of the top differentially expressed genes upon DBZ treatment in *Pten*-positive lymphoblasts that are rescued by *Pten* loss. *P* values (**c**,**e**) were calculated using two-tailed Student's t-test. Bar graphs indicate mean ± s.d. (n = 3 for *Pten*$^{-/-}$ groups and n = 6 for *Pten*$^{+/+}$ groups).

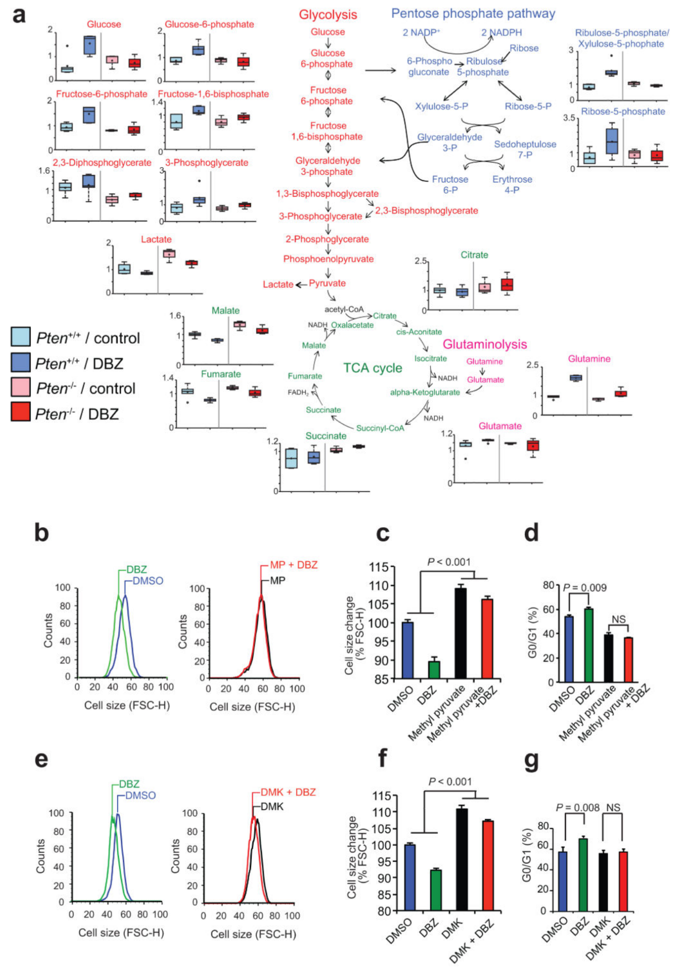

Figure 2.

Metabolic profiling analysis and metabolic rescue of NOTCH1 inhibition in T-ALL. (**a**) GC/MS and LC/MS/MS metabolic profiles (mass spectrometry scaled intensity) of DBZ-treated mice harboring *Pten*-positive or *Pten*-deleted isogenic leukemias. Changes in glycolysis, pentose phospate pathway, glutaminolysis and TCA cycle intermediates are shown (scaled intensity arbitrary units). Box plots represent the upper quartile to lower quartile distribution. + Sign indicates mean value and horizontal line the median value. Whiskers indicate the maximum and minimum values of the distribution. Open circles indicate extreme data points. (n = 3 for $Pten^{-/-}$ groups and n = 6 for $Pten^{+/+}$ groups). (**b**,**c**) Representative flow cytometry histograms (**b**) and quantitative analyses (**c**) showing cell diameter changes induced by DBZ treatment in DND41 cells treated with DMSO only or DBZ, in the presence or absence of methyl pyruvate. (**d**) Cell cycle analysis of DND41 cells treated with vehicle only or DBZ, in the presence or absence of methyl pyruvate. (**e**,**f**) Representative flow cytometry histograms (**e**) and quantitative analyses (**f**) showing cell diameter changes induced by DBZ treatment in DND41 cells treated with DMSO only or DBZ, in the presence or absence of dimethyl ketoglutarate. (**g**) Cell cycle analysis of DND41 cells treated with DMSO only or DBZ, in the presence or absence of dimethyl ketoglutarate. MP= methyl pyruvate; DMK= dimethyl ketoglurate. *P* values were calculated using two-tailed Student's t-test. Bar graphs indicate mean ± s.d of biological triplicates.

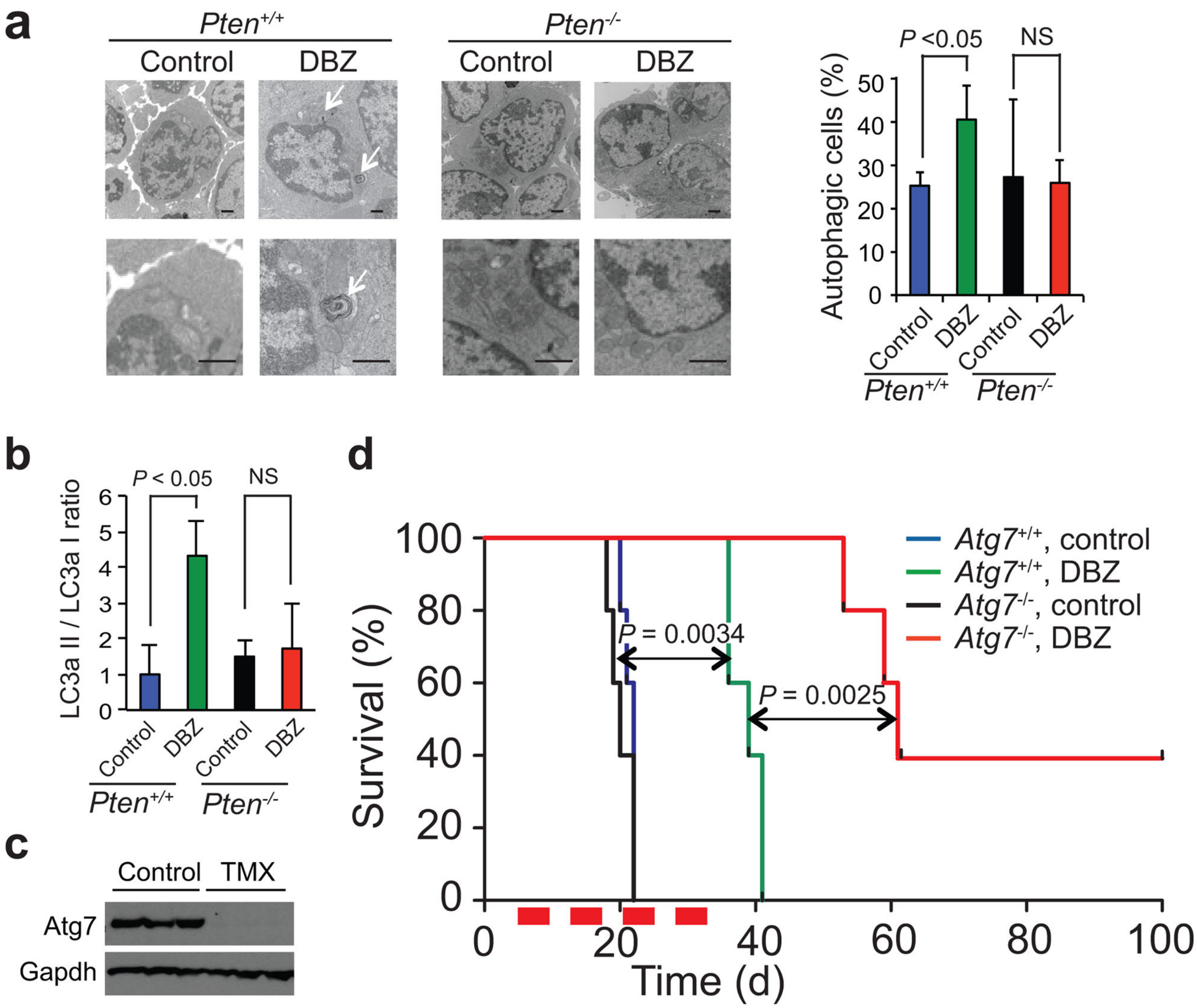

Figure 3.

Autophagy supports leukemia cell growth in response to NOTCH1 inhibition. (**a**) Representative images of electron microscopy micrographs of *Pten*-positive and *Pten*-deleted lymphoblasts acutely treated with vehicle only or DBZ *in vivo*. Quantification of the percentage of cells with autophagosomes is shown on the right (n = 3 per group). (**b**) Quantification of LC3a II / LC3a I protein ratio after acute treatment of leukemic mice with vehicle only or DBZ. *P* values were calculated using two-tailed Student's t-test. Bar graphs indicate mean ± s.d. (n = 3 per group) (**c**) Western blot analyses showing Atg7 expression in *Rosa26*$^{Cre\text{-}ERT2/+}$ *Atg7*$^{f/f}$ leukemias treated with tamoxifen. (**d**) Kaplan-Meier survival curve of mice harboring *Atg7*-positive and *Atg7*-deleted isogenic leukemias treated with 4 cycles of vehicle or DBZ (5 mg Kg^{-1}) on a 4 days ON (red blocks) and 3 days OFF schedule (n = 5 per group). Scale bars, 500 nm (**a**).

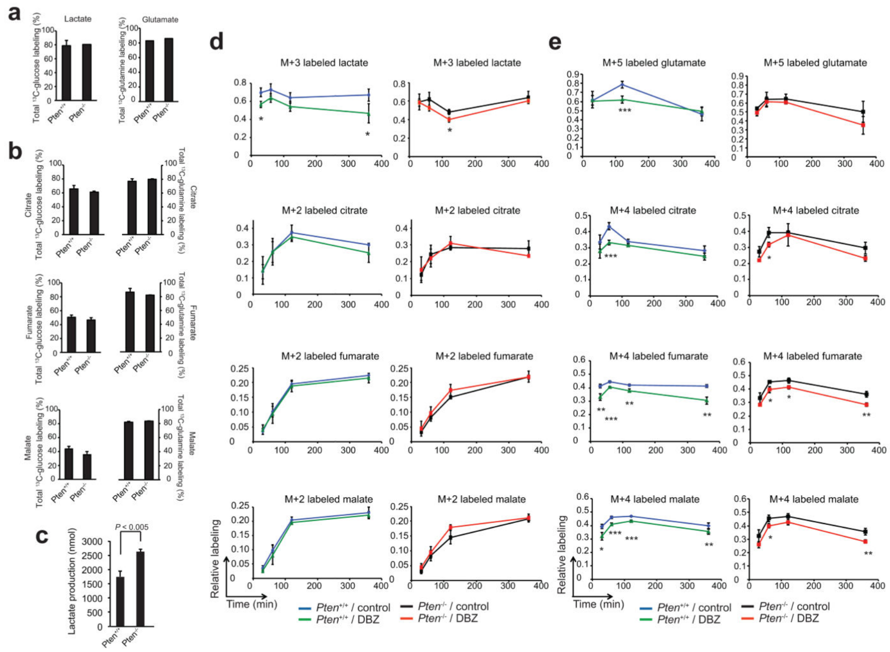

Figure 4.

Glucose and glutamine metabolic flux analysis of T-ALL cells upon NOTCH1 inhibition and *Pten* loss. (**a**) Percentage of ^{13}C incorporation into lactate and glutamate after incubation of primary NOTCH1-induced T-ALL cells with ^{13}C-glucose and ^{13}C-glutamine, respectively. (**b**) Percentage of ^{13}C incorporation into TCA cycle intermediates after incubation of primary NOTCH1-induced T-ALL cells with ^{13}C-glucose and ^{13}C-glutamine, respectively. (**c**) Extracellular levels of lactate produced by *Pten*-positive and *Pten*-deleted leukemia cells after 6 hours of culture *in vitro* using dialyzed medium. (**d**) Kinetic analysis of glucose incorporation in primary lymphoblasts incubated with ^{13}C-glucose. (**e**) Kinetic analysis of glutamine incorporation in primary lymphoblasts incubated with ^{13}C-glutamine. M+2, +3, +4 or +5 labeled compounds indicate molecules of those compounds that contain 2, 3, 4 or 5 ^{13}C atoms, respectively. Bar graphs and kinetic curves indicate mean ± s.d. *P* values were calculated using Student's t-test between control and DBZ treated samples across all time points (****P* < 0.005; ***P* < 0.01; **P* < 0.05; n = 3 per group).

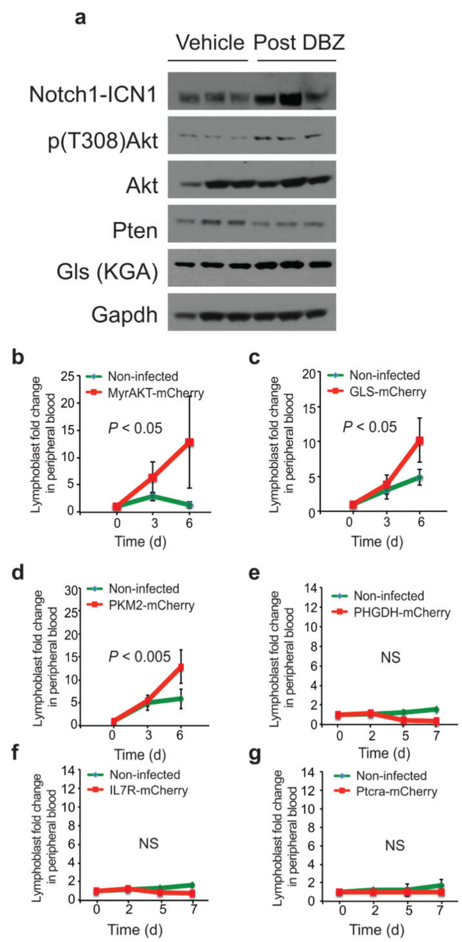

Figure 5.

Rescue of GSI antileukemic effects in *Pten*-positive leukemias. (**a**) Western blot analyses showing intracellular activated NOTCH1, p(T308) Akt, Akt total, Pten and Gls expression in *Pten*-positive leukemias progressing after 4 cycles of treatment with vehicle or DBZ (5 mg Kg^{-1}) on a 4 days ON (red blocks) and 3 days OFF schedule. (**b-g**) Peripheral blood leukemia infiltration in mice harboring NOTCH1-induced *Pten*-positive T-ALL cells expressing (**b**) MyrAKT plus mCherry, (**c**) Glutaminase plus mCherry, (**d**) PKM2 plus mCherry, (**e**) PHGDH plus mCherry (**f**) IL7R plus mCherry or (**g**) preTCRalpha (Ptcra) plus mCherry, upon treatment with DBZ. Changes in leukemia cell counts of non-infected (mCherry negative) cells are shown as internal control. Graphs indicate median ± s.d. *P* values were calculated using two-tailed Student's t-test (n = 5 mice per group).

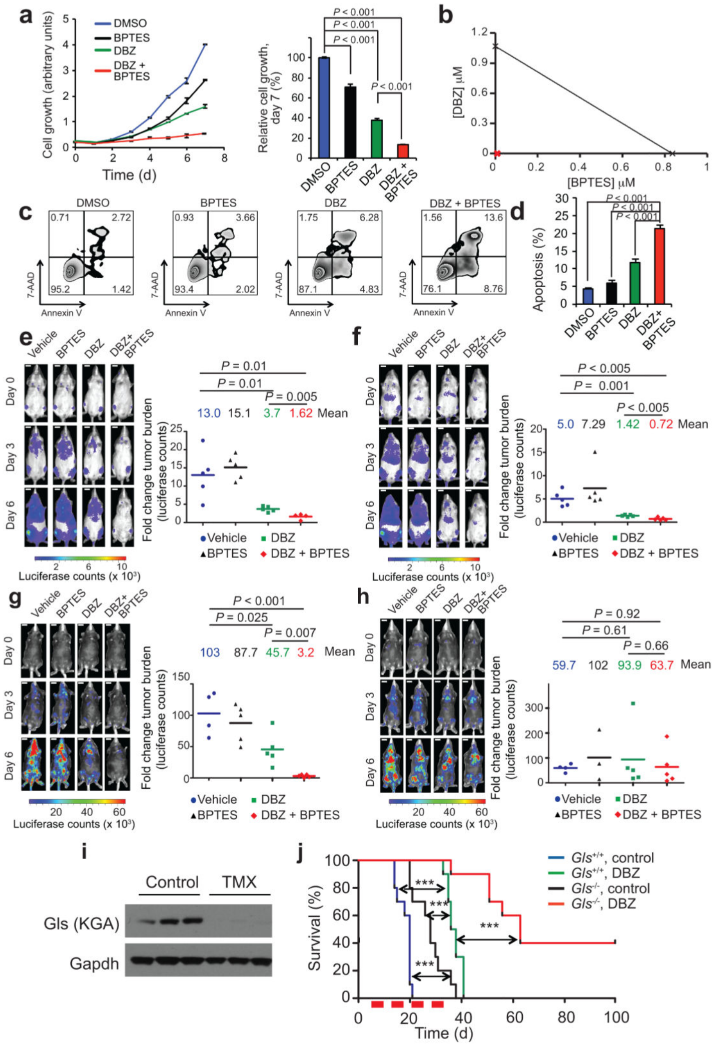

Figure 6.

Synergistic antileukemic effects of glutaminase inhibition and GSI treatment in T-ALL. (**a**) Differential growth of HPB-ALL cells treated with DMSO, DBZ, BPTES, or DBZ plus BPTES combination *in vitro*. (**b**) Isobologram analysis of DBZ plus BPTES combination in HPB-ALL cells. X shape mark in red shows value for combination index at ED50. (**c,d**) Representative flow cytometry plots of Annexin V/7AAD staining (**c**) and quantitation of apoptosis (**d**) of HPB-ALL cells treated with the different drug combinations. (**e,f**) Representative images (left) and quantitation (right) of tumor burden changes assessed by bioimaging in mice xenografted with human primary T-ALL cells PDTALL#19 (**e**) or PDTALL#10 (**f**) treated with the different drug combinations (n = 5 per group except PDTALL#19 DBZ+BPTES, n = 4). (**g,h**) Representative images (left) and quantitation (right) of tumor burden changes assessed by bioimaging in mice allografted with *NOTCH1*-induced *Pten*-positive (**g**) or *Pten*-deleted (**h**) mouse leukemia lymphoblasts treated with the different drug combinations (n = 5 per group except: $Pten^{-/-}$/Vehicle, n = 4; $Pten^{-/-}$/BPTES, n = 3). (**i**) Western blot analyses showing Gls expression in $Rosa26^{Cre\text{-}ERT2/+}$ $Gls^{f/f}$ leukemias treated with vehicle or tamoxifen. (**j**) Kaplan-Meier survival curve of mice harboring *Gls*-positive and *Gls*-deleted isogenic leukemias treated with 4 cycles of vehicle or DBZ (5 mg Kg^{-1}) on a 4 days ON (red blocks) and 3 days OFF schedule (****P* < 0.005; n = 10 per group). *P* values (**a**,**d**) were calculated using two-tailed Student's t-test. Bar graphs indicate mean ± s.d. of biological triplicates. Scale bars, 1 cm (**e–h**).